Phonon drag as a mechanism of delayed terahertz response of metals

Ivan Oladyshkin*

Department of Nonlinear Electrodynamics, A.V. Gaponov-Grekhov Institute of Applied Physics of the Russian Academy of Sciences, 603950, 46 Ul'yanov Street, Nizhny Novgorod, Russia

(Received 16 April 2026; accepted 17 August 2026; published 2 September 2026)

We show that electron drag by nonequilibrium phonons describes the actual duration and spectrum of terahertz pulses generated during femtosecond laser irradiation of metals. In contrast to previous models, there is a picosecond delay in the drag force development due to the relatively slow lattice heating and finite phonon lifetime. We also predict that at high pump fluences a macroscopic deformation wave nonlinearly enhances the drag force and terahertz response. Our results establish the terahertz pulse wave form as a direct probe of ultrafast lattice dynamics in metals.

DOI: 10.1103/qz25-c2fq

I. INTRODUCTION

Despite significant advances in coherent phonon control, probing ultrafast lattice dynamics in solids on picosecond timescales with conventional methods remains nontrivial. In this paper we show that laser-induced terahertz emission from metals offers a direct window into these processes. We demonstrate that the observed characteristics of terahertz pulses can be explained by the phonon-drag force—the delayed transfer of phonon momentum to electrons—which naturally imprints the thermal evolution of the crystal lattice onto the emitted radiation. This makes the terahertz signal a quantitative probe of picosecond dynamics of heat flux or macroscopic deformation wave at high pump fluences.

Previous attempts to interpret the terahertz response of metals [1–5] have failed to explain the essential features of this effect from a microscopic point of view. The key problem is the universally delayed character of the terahertz signal: a femtosecond laser pump generates a much longer low-frequency pulse with a duration of 1–2 ps and a spectral range of 0.3–2 THz [6–13].

In experimental papers [6–8], where optical-to-terahertz conversion on metal surfaces was first observed, only a phenomenological description of this effect was provided in terms of nonlinear susceptibility χ_2. The first microscopic models [1–3], based on the ponderomotive effect, significantly underestimated the actual terahertz amplitude and predicted direct laser pulse rectification, which contradicted experimental observations. Subsequent microscopic models invoked the gradient of hot-electron pressure and the photon drag force as the terahertz radiation sources [3–5]. These two sources are comparable in magnitude [5] and significantly exceed the ponderomotive force. Despite a slight delay in electron temperature dynamics, the predicted terahertz signal, however, was still close to the laser pulse envelope.

Nevertheless, a noticeable outcome of these studies is the introduction of a Cherenkov interaction geometry for the case of oblique pump incidence, when a terahertz field is generated by a light spot moving along the metal surface at a superluminal phase velocity (see Fig. 1). This framework successfully explained the terahertz radiation direction coinciding with the pump reflection. Also, in these papers several electrodynamical problems of low-frequency radiation from various nonlinear sources were solved that will be used in the present work in a generalized form.

II. PHONON-DRAG FORCE

The models discussed above assumed that free electrons experience a classical "viscous friction" force from the crystal lattice and that momentum transferred to the lattice is irreversibly lost. This assumption is, however, generally invalid: upon collision, electron momentum is transferred to the phonon subsystem and may, with a certain probability, return to the electronic subsystem via subsequent collisions. Phenomena of this kind are termed *phonon wind* or *phonon drag* when they involve the exchange of directed momentum, and *thermal drag* when the force originates from a temperature gradient in the phonon gas [14,15]. The eventual dissipation of momentum of the electron–phonon system occurs only on picosecond timescales, predominantly through Umklapp phonon scattering (U-processes), whereby momentum is transferred to the crystal lattice as a whole. In stationary regimes, *e-ph* momentum exchange merely renormalizes the effective electron–phonon collision frequency. But on picosecond timescales, when the two subsystems are far from equilibrium, momentum exchange can induce a pronounced temporal dispersion of the electronic response.

Consider the phonon-drag effect in the case when the crystal lattice of metal is nonuniformly heated due to the laser pulse absorption. There is a directed phonon flux that transports heat away from the near-surface layer, and the momentum of phonons can be transferred to electrons during collisions. To make preliminary estimates, we assume the

*Contact author: oladyshkin@ipfran.ru

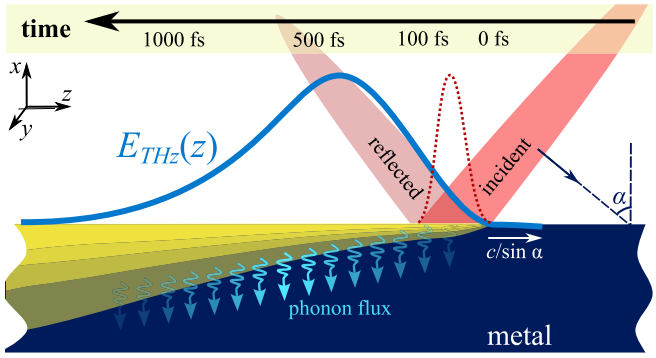

FIG. 1. Schematic of phonon-driven terahertz generation. The yellow gradient is the lattice temperature distribution; wavy blue arrows depict the phonon flux. The thick blue curve shows the terahertz field $E_z(z)$, produced by phonon drag at the metal surface, while the dotted red curve is the laser pulse envelope. The timeline at the top marks the time after the pump arrival.

diffusive regime of heat transport, when the phonon heat flux, $\mathbf{\Pi}_{\rm ph}$, is governed by Fourier's law [16]:

$$\mathbf{\Pi}_{\rm ph} = -\varkappa_l \nabla T_l, \tag{1}$$

where $\varkappa_l$ and T_l are the crystal lattice thermal conductivity and temperature, respectively. Microscopically, the energy flux $\mathbf{\Pi}_{\rm ph}$ is created by propagating acoustic phonons with the dispersion law $\omega = qc_s$, where q and ω are the phonon wave number and frequency, respectively, and c_s is the sound velocity. Here we neglect the differences in sound velocity among the various phonon modes and deviations from linear dispersion, as they are presently inessential. In this case the energy of a phonon $\hbar\omega$ is linearly related to its momentum $p_{\rm ph}$ as $\hbar\omega = p_{\rm ph}c_s$, so that the total energy flux carried by phonons is linearly related to their macroscopic momentum per unit volume $\mathbf{P}_{\rm ph}$: $\mathbf{\Pi}_{\rm ph} = c_s^2\mathbf{P}_{\rm ph}$.

Introducing the phonon-electron scattering rate $\nu_{{\rm ph}-e}$ (the frequency of momentum transfer from phonons to electrons), we can express the phonon-drag force per unit volume, $\mathbf{F}_{\rm ph}$:

$$\mathbf{F}_{\rm ph} = \nu_{{\rm ph}-e}\mathbf{P}_{\rm ph} = -\frac{\varkappa_l \nu_{{\rm ph}-e}}{c_s^2}\nabla T_l. \tag{2}$$

This relation between the directed phonon flux and the lattice temperature gradient also follows from the standard kinetic theory of phonon transport [14], which reduces to Fourier's law in the diffusive limit.

According to Eq. (2), the temporal evolution of the drag force depends directly on the dynamics of the crystal lattice temperature, and so, it does not follow the laser pulse envelope. In the relaxation-time approximation, the lattice thermal conductivity takes the standard form [16]:

$$\varkappa_l = \frac{c_s^2}{3\nu_{\rm ph}}C_l, \tag{3}$$

where $\nu_{\rm ph}$ is the total scattering frequency of phonons, and C_l is the heat capacity of the crystal lattice per unit volume. Therefore we obtain

$$\mathbf{F}_{\rm ph} = -\frac{1}{3}\frac{\nu_{{\rm ph}-e}}{\nu_{\rm ph}}\nabla U_l, \tag{4}$$

where $U_l = C_l T_l$ is the thermal energy of the crystal lattice. The ratio $\nu_{{\rm ph}-e}/\nu_{\rm ph}$ quantifies the fraction of the phonon momentum that is returned to the electrons and typically lies in the range of 0.1–0.9, depending on the strength of electron–phonon coupling in a specific metal [17,18].

Equation (4) allows us to compare directly the phonon-drag force with the electronic pressure gradient $\mathbf{F}_e$ [19], which was considered as a source of terahertz radiation in previous models [4,5]:

$$\mathbf{F}_e = -\frac{2}{3}\nabla U_e, \tag{5}$$

where U_e is the average kinetic energy of electrons per unit volume. One can see that $\mathbf{F}_{\rm ph}$ and $\mathbf{F}_e$ have similar gradient form, and their amplitudes depend on the distribution of thermal energy between the electrons and the crystal lattice.

At the initial stage of interaction, the laser pulse energy is deposited in the electron subsystem so that initially $\mathbf{F}_e$ will exceed $\mathbf{F}_{\rm ph}$, especially if the heat exchange between electrons and crystal lattice is slow (like in Au). During further thermalization almost all absorbed energy will be transferred to the crystal lattice, since its heat capacity is much larger than the heat capacity of electron gas. At this stage the phonon-drag force (4) will exceed electronic pressure (5) by a factor of several to several tens, depending on $\nu_{{\rm ph}-e}/\nu_{\rm ph}$. In metals with strong electron–phonon coupling and fast thermalization (like Fe, Ni, Co), the phonon-drag force is expected to exceed the electronic pressure force even during the laser pulse action.

Introduction of the phonon-drag force $\mathbf{F}_{\rm ph}$, which is substantially delayed relative to the laser pump, allow us, in principle, to interpret the actual wave forms of terahertz pulses. However, aiming to correctly describe the phonon flux dynamics at picosecond timescales, we need to improve the model of phonon transport. The classical heat conductivity model, used for the above estimates, assumes that the energy flux (1) appears instantaneously with the lattice temperature gradient. But it is valid only at timescales larger than the time of phonon mean free path $\tau_{\rm ph} = \nu_{\rm ph}^{-1}$, which is typically equal to several picoseconds [17,18,20]. At shorter timescales, the finite phonon lifetime $\tau_{\rm ph}$ cannot be neglected.

To account for the finite phonon lifetime, we employ the Boltzmann kinetic equation for the phonon distribution function. Following the standard moment method in the relaxation-time approximation [14] and retaining the explicit time derivatives essential for the picosecond dynamics, we obtain the following equations for the total phonon momentum $\mathbf{P}_{\rm ph}(\mathbf{r}, t)$ and total phonon energy $U_l(\mathbf{r}, t)$ per unit volume (see the derivation in Appendix A):

$$\frac{\partial \mathbf{P}_{\rm ph}}{\partial t} + \frac{1}{3}\nabla U_l = -\nu_U \mathbf{P}_{\rm ph} - \nu_{{\rm ph}-e}\mathbf{P}_{\rm ph} + \nu_{e-{\rm ph}}\mathbf{P}_e, \tag{6}$$

$$\frac{\partial U_l}{\partial t} + c_s^2 \,{\rm div}\, \mathbf{P}_{\rm ph} = S_e, \tag{7}$$

where S_e describes the crystal lattice heating by electrons, $\mathbf{P}_e$ is the momentum of electrons per unit volume, ν_U is relaxation rate due to U processes, and $\nu_{e-{\rm ph}}$ and $\nu_{{\rm ph}-e}$ are the frequencies of e-ph and ph-e collisions, respectively. The frequencies $\nu_{e-{\rm ph}}$ and $\nu_{{\rm ph}-e}$ obey the balance relation $\nu_{e-{\rm ph}}n_e = \nu_{{\rm ph}-e}n_{\rm ph}$, where $n_{\rm ph}$ and n_e are the concentrations of phonons and free electrons, respectively. At room temperature $n_{\rm ph}$ exceeds n_e

by 1–2 orders of magnitude, so the phonon lifetime is much larger than the electron free path time. In the limit of the stationary heat flux, when $\partial/\partial t$ is much smaller than the phonon relaxation rate $\nu_U + \nu_{\mathrm{ph}-e}$ and when the electron current is zero (i.e., $\mathbf{P}_e = 0$), Eqs. (6) and (7) transform into the classical diffusion equation for the crystal lattice temperature, with the heat conductivity given by Eq. (3) and the source S_e.

In contrast to quasistationary treatments of phonon drag, the full system of Eqs. (6)–(7) captures the transient buildup of the phonon flux, which is responsible for the delayed terahertz response. According to these equations, the phonon flux does not arise instantaneously with the crystal lattice heating, while its growth rate is proportional to the gradient of the lattice thermal energy ∇U_l. The stationary flux is established during the time $t_{\mathrm{ph}} \approx (\nu_U + \nu_{\mathrm{ph}-e})^{-1}$, i.e., in a picosecond timescale. At timescales $t \gg t_{\mathrm{ph}}$, this system describes the classical regime of diffusive thermal conductivity.

The relaxation rates $\nu_{e-\mathrm{ph}}$, $\nu_{\mathrm{ph}-e}$, and ν_U are, in general, mode and temperature dependent [17,18,20]. For example, hot electrons primarily excite longitudinal acoustic (LA) phonons, while transverse acoustic (TA) phonons are populated indirectly via anharmonic decay on a timescale of ∼0.2–0.5 ps [20]. The full thermalization of the phonon subsystem and the corresponding dissipation of the directed phonon momentum occurs within 1–3 ps due to Umklapp scattering. This naturally introduces the picosecond delay required to explain the observed terahertz pulse durations.

Since the phonon-drag effect is an integral characteristic of the phonon distribution, and since for acoustic phonons the energy–momentum relation is linear ($\omega = qc_s$), the total momentum $\mathbf{P}_{\mathrm{ph}}$ transferred to electrons depends only on the integrated energy flux, not on its mode composition. That is why here we use the two-temperature model for S_e [21,22], assuming that the heat flux arises on the background of locally thermalized distribution of phonons f_0 with the temperature T_l. As it was recently demonstrated [17], the two-temperature model accurately captures the integrated energy exchange between the electrons and the crystal lattice.

Regarding the temperature dependence, in the low-fluence regime (the main focus of Secs. II and III) the lattice temperature increase is modest ($\Delta T_l \lesssim 100$ K), so the rates can be treated as constants. At high fluences (Sec. IV), the phonon distribution becomes strongly nonthermal and the dynamics are dominated by the coherent deformation wave; in that regime, we rely on macroscopic mechanical parameters rather than on microscopic rates in our estimations.

In the two-temperature model, the energy transfer from the electrons to the crystal lattice is described by the following equation:

$$S_e = \mathrm{G}C_e(T_e - T_l), \tag{8}$$

where $C_e \cong n_e \frac{\pi^2}{2}\frac{k^2 T_e}{E_F}$ is the heat capacity of degenerate electron gas per unit volume [19] (k is the Boltzmann constant, E_F is the Fermi energy), and G is the temperature relaxation rate. For the evolution of electron temperature, we can write the diffusion-type equation [21,22]:

$$\frac{\partial T_e}{\partial t} = D_e \frac{\partial^2 T_e}{\partial x^2} - \mathrm{G}(T_e - T_l) + \frac{n_e e^2 E_{\mathrm{opt}}^2}{C_e\left(\nu_e^2 + \omega^2\right)}\nu_e, \tag{9}$$

where D_e is the electron thermal diffusivity, e is the electron charge, ν_e is the total collision frequency of electrons, ω is the laser pulse frequency, and E_{opt} is the amplitude of the optical field inside the metal (decaying exponentially on the scale of the skin depth). Here D_e can be expressed as $D_e = v_{\mathrm{F}}^2/3\nu_e$, where v_{F} is the Fermi velocity [16]. The last term in Eq. (9) expresses the absorbed power density, derived from the Drude model as the work of the optical field on electrons [23], while the term $\mathrm{G}(T_e - T_l)$ describes the heat transfer to the crystal lattice.

Finally, to close the system, we add the equation of low-frequency electron motion:

$$\frac{\partial \mathbf{P}_e}{\partial t} = -en_e\mathbf{E} + \nu_{\mathrm{ph}-e}\mathbf{P}_{\mathrm{ph}} - \nu_{e-\mathrm{ph}}\mathbf{P}_e, \tag{10}$$

where $\mathbf{E}$ is the self-consistent low-frequency electric field inside the metal. The terms $\nu_{\mathrm{ph}-e}\mathbf{P}_{\mathrm{ph}}$ and $\nu_{e-\mathrm{ph}}\mathbf{P}_e$, which appear symmetrically in Eqs. (6) and (10), describe the drag force between the electrons and phonons.

For brevity, we do not include the gradient of electron pressure in Eq. (10), since the problem of radiation from this source has already been solved [4,5] (see also Appendix B). We also omit explicit treatment of electron collisions with impurities and defects, since electron–phonon scattering dominates at room temperature and above (so that ν_e is close to $\nu_{e-\mathrm{ph}}$). Finally, we neglect e-e Umklapp scattering, which contributes significantly to momentum dissipation only when the electron temperature is comparable with the Fermi energy.

The numerical values of the relaxation rates used in the calculations below are taken from the recent theoretical papers [17,18,20] and varied in physically reasonable ranges. For gold we use the basic value of $\mathrm{G} = 2 \times 10^{12}$, corresponding to an electron–phonon thermalization time of ~ 0.5 ps, consistent with first-principles calculations at elevated electron temperatures [17,20]. The total phonon damping rate is varied in the range $\nu_{\mathrm{ph}} = (1 \div 5) \times 10^{12}\ \mathrm{s}^{-1}$, which matches the calculated lifetimes of transverse acoustic phonons in Au [20] (since TA phonons make the main contribution to the phonon-drag effect).

III. LOW-FREQUENCY RADIATION

To relate the resulting model to the terahertz emission, one must solve the problem of radiation from electrons driven by the phonon-drag force. Similar problems for various sources have already been thoroughly analyzed in [1–5]; the relevant results are summarized in Appendix B. Briefly, because the plasma frequency in metals is extremely high ($\sim 10^{16}\ \mathrm{s}^{-1}$), any potential force acting on the electron subsystem is screened almost instantaneously by charge-separation field $\mathbf{E}$ (with rot $\mathbf{E} \cong 0$, since the field is quasistatic). Consequently, the electric current is negligible, so that $\mathbf{P}_e \cong 0$. Radiation from this system arises solely due to the presence of the boundary and the slow variations of the quasistatic fields.

The phonon-drag force $\mathbf{F}_{\mathrm{ph}} = \nu_{\mathrm{ph}-e}\mathbf{P}_{\mathrm{ph}}$, driven by inhomogeneous heating of the crystal lattice, is also a potential force and is therefore compensated by a quasistatic charge-separation field $\mathbf{E}$ inside the metal:

$$en_e\mathbf{E} = \nu_{\mathrm{ph}-e}\mathbf{P}_{\mathrm{ph}}. \tag{11}$$

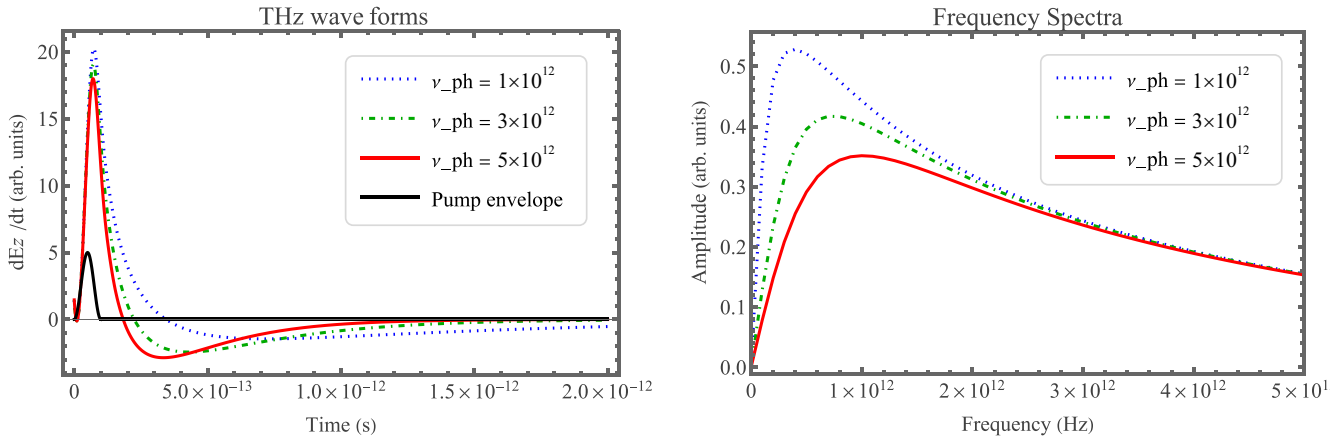

FIG. 2. Wave forms of terahertz pulses in the far-field zone $dE_z(t)/dt$ (left panel) and their spectra (right panel) calculated for the parameters of gold. Solid black curve on the left panel is the laser pulse envelope (FWHM is equal to 50 fs). Material parameters used in the modelling: $G = 2 \times 10^{12}\ \mathrm{s}^{-1}$, $\nu_e = 2 \times 10^{14}\ \mathrm{s}^{-1}$, and the phonon damping rate ν_{ph} is $(1 \div 5) \times 10^{12}\ \mathrm{s}^{-1}$.

Using this relation, one can rewrite Eq. (6) as the equation on $\mathbf{E}$:

$$\frac{\partial \mathbf{E}}{\partial t} + \nu_{\mathrm{ph}}\mathbf{E} = -\frac{\nu_{\mathrm{ph}-e}}{3en_e}\nabla U_l, \tag{12}$$

where $\nu_{\mathrm{ph}} = \nu_{\mathrm{ph}-e} + \nu_U$ is the total collision rate of phonons. Equation (12) gives an analytical solution for the electric field $\mathbf{E}$:

$$\mathbf{E}(\mathbf{r}, t) = -\frac{1}{3}\frac{\nu_{\mathrm{ph}-e}C_l}{en_e}\int_{-\infty}^{t} \nabla T_l(\mathbf{r}, t')\mathrm{e}^{\nu_{\mathrm{ph}}(t'-t)}dt'. \tag{13}$$

In its spatial structure, $\mathbf{E}(\mathbf{r}, t)$ resembles that of an electrical double layer with a time-varying surface charge $\sigma(z, t)$. The normal component of the field is localized inside the metal: at the boundary $E_x = 0$ since $\frac{\partial T_l}{\partial x} = 0$ (no heat flux across the surface). The tangential component E_z, however, is nonzero and continuous across the boundary, so it can be used to find low-frequency radiation.

The most transparent analytical solution can be obtained for the Cherenkov geometry, which is typical for real experiments. Consider a laser pulse obliquely incident on the metal at an angle α so that the terahertz signal is generated within a narrow interaction region that moves along the surface with a superluminal phase velocity $c/\sin\alpha$ (see Fig. 1). If the laser spot diameter is large compared to the terahertz wavelength, all distributions become stationary in the reference frame comoving with the interaction region. Mathematically, this translates into the relation $\frac{\partial}{\partial t} = -\frac{c}{\sin\alpha}\frac{\partial}{\partial z}$.

Under these conditions, Eq. (13) yields the following expression:

$$E_z(t) = \frac{\sin\alpha}{c}\frac{\nu_{\mathrm{ph}-e}C_l}{3en_e}\int_{-\infty}^{t}\frac{\partial T_l}{\partial t'}\mathrm{e}^{\nu_{\mathrm{ph}}(t'-t)}dt', \tag{14}$$

which gives the explicit relation between the tangential low-frequency electric field and the "history" of the crystal lattice temperature $T_l(\mathbf{r}, t')$ at a given point, including the metal boundary $x = 0$.

There are two important limits of Eq. (14). If the phonon relaxation time, ν_{ph}^{-1} is much larger than the characteristic time of lattice temperature variation; we obtain $E_z \propto (T_l(t) - T_0)\mathrm{e}^{-\nu_{\mathrm{ph}}t}$, where T_0 is the initial lattice temperature. In the opposite case $E_z \propto \frac{1}{\nu_{\mathrm{ph}}}\frac{\partial T_l(t)}{\partial t}$, which corresponds to the diffusion limit [Eqs. (2) and (3)]. Thus the phonon-drag force produces a terahertz pulse with the wave form determined by the dynamics of the crystal lattice temperature $T_l(t)$ and by the relaxation of phonons. Under the chosen geometry of oblique incidence, the magnetic field H_y on the metal surface is given by $H_y = -E_z/\cos\alpha$, which allows us to find the Poynting vector and calculate the total terahertz pulse energy for given size of the laser spot.

The results presented in Figs. 2 and 3 were obtained by numerical solution of the coupled system of Eqs. (6), (7), (9), and (11), with the far-field wave form computed from Eq. (14). The normalized pump envelope is also provided for comparison. In the numerical modeling, we use the full Drude expression for the absorbed power [last term in Eq. (9)], including the Fresnel transmission coefficient and the spatial profile $E_{\mathrm{opt}}(x) \propto \exp(x/l_{sk})$. The pulse envelope is explicitly included as $\sin^2(\pi t/\tau_p)$, where τ_p is the full pump pulse duration. The prefactors are chosen consistently with the Drude model; however, since the wave forms and spectra in Figs. 2 and 3 are normalized to their respective maxima, the absolute amplitude of the optical field does not affect the temporal shape of the terahertz response. For further high-fluence estimates in Sec. IV, we use independent macroscopic values that do not rely on these prefactors.

Depicted graphs of dE_z/dt describe the terahertz signal wave forms in the far-field zone, and the chosen range of $\nu_{\mathrm{ph}} = (1 \div 5) \times 10^{12}\ \mathrm{s}^{-1}$ corresponds to the lifetime of TA phonons, which is 0.2–1 ps, according to calculations from Ref. [20]. As Fig. 2 shows, the phonon-drag mechanism predicts terahertz pulses of picosecond duration, with the spectral maximum in the range of 0.3–1 THz, depending on the phonon relaxation rate ν_{ph} and the electron-lattice thermalization rate G.

The previous models of terahertz generation, based on purely electronic response (ponderomotive force, photon drag, or electronic pressure), predicted terahertz pulses with the duration and spectrum close to the laser pulse envelope. But the spectrum of the pump envelope is typically peaked at a frequency ~10 THz, which is about 10 times higher than the

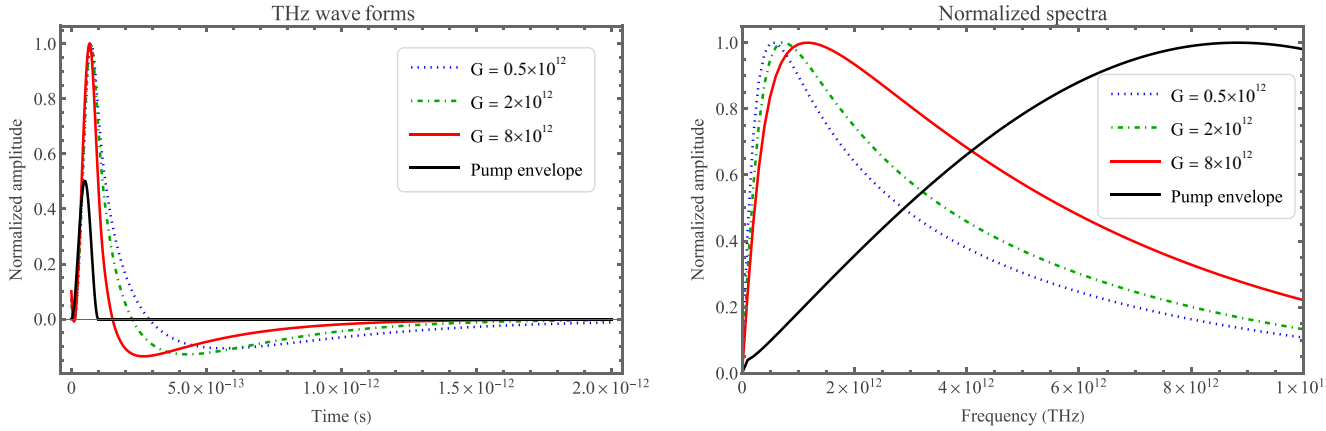

FIG. 3. Normalized wave forms of terahertz pulses in far-field zone $dE_z(t)/dt$ (left panel) and their spectra (right panel) calculated for the phonon damping rate $\nu_{\rm ph} = 3 \times 10^{12}\,{\rm s}^{-1}$ and various electron-lattice thermalization constants $G = \{0.5,\ 2,\ 8\} \times 10^{12}\,{\rm s}^{-1}$; the other parameters are the same as in Fig. 2. The solid black curve on the right panel shows the spectrum of the pump envelope, which is peaked at ∼10 THz, i.e., an order of magnitude higher than the terahertz signal peaks (0.3–1.5 THz).

spectral peak of terahertz signals, measured experimentally and predicted by the phonon-drag model (see right panel of Fig. 3 and Table I for comparison).

Figure 3 illustrates the dependence of the terahertz signal wave form on the electron-lattice relaxation rate G. Figures 2 and 3 show that the roles of parameter G and the phonon relaxation rate $\nu_{\rm ph}$ are similar: they determine the buildup and decay time of the phonon wind and therefore affect the spectrum of the generated terahertz radiation in a comparable way. Their increase shortens the signal duration and shifts the spectral maximum toward higher frequencies (but still not higher than ∼1.5 THz).

At the same time, variations of the electron collision frequency ν_e within reasonable limits of 10^{14}–$10^{15}\,{\rm s}^{-1}$ (and corresponding variations of the diffusivity D_e) have a rather weak effect on the resulting terahertz signal. In this range the heat diffusion from the skin layer is faster than other relaxation processes, so that the phonon pressure dynamics is determined mainly by the relaxation rates G and $\nu_{\rm ph}$, rather than by electronic diffusion.

Passing to more detailed discussion of experimentally measured terahertz signals, we should note that their direct comparison with the theoretically predicted ones is strongly limited by the spectral characteristics of terahertz detectors. The experimental schemes for terahertz wave-form reconstruction with nonlinear crystals usually have a frequency limit of about 1.5–2 THz, so that they miss high-frequency components of the signal and, consequently, sharp rising edges in the terahertz wave form. This comes mostly from the velocity mismatch between optical and terahertz pulses and phonon absorption in the nonlinear crystals used as detectors.

In Table I the experimental results on the laser-induced terahertz generation from flat metal surfaces and gratings are summarized. The duration of the main oscillation in the terahertz signal is provided separately, since residual terahertz oscillations are commonly associated with multiple reflections, water vapor reemission, and other parasitic effects. These data show that the detected terahertz signal is undoubtedly much longer than the pump pulse, but its duration and spectral maximum significantly vary depending on the sample parameters and, apparently, detection scheme. According to the cited papers [6–9,12,13,24,25], no spectral calibration or deconvolution of the detector response has been performed in these studies. The quantities that can be reliably extracted from the available data are the typical pulse duration (0.5–1.5 ps) and the spectral peak position (0.3–1.5 THz), which

TABLE I. Characteristics of the terahertz pulses observed during femtosecond laser irradiation of flat metal surfaces and gratings. Notes: (1) in paper [24] (row 6), several pump pulse durations were used, and the significant shift of the terahertz spectral maximum was observed for the pump duration of 980 fs; (2) in paper [25] (row 7), the terahertz radiation was generated by a two-color pump.

	Sample	Duration of the first oscillation	Spectral maximum	Pump	References
1	Flat Au film, 100 nm	1.5 ps	–	810 nm, 50 fs	Kadlec, 2004 [7]
2	Flat Au films, < 260 nm	–	0.3 THz	810 nm, 50 fs	Kadlec, 2005 [8]
3	Flat Fe film, 12 nm	4–5 ps	0.2 THz	800 nm, 50 fs	Hilton, 2004 [6]
4	Au grating, 30 nm	1.5 ps	0.75 THz	800 nm, 100 fs	Welsh, 2007 & Welsh 2009 [12,13]
5	Au grating, 100 nm	0.2–0.8 ps	–	800 nm, 50 fs	Ramanandan, 2014 [9]
6	Bi, bulk	–	∼ 0.6 THz	790 nm, 50–225 fs	Ilyakov, 2016 [24]
			∼ 0.3 THz	790 nm, 980 fs	
7	Flat Au films, 5–30 nm	0.75 ps	0.75–1.6 THz	800 nm + 400 nm, 50 fs	Dai, 2014 [25]

are in good agreement with the theoretical predictions of the phonon-drag model.

We also note that the enhanced terahertz emission observed from grating-structured surfaces [9,12,13] is naturally explained by the resonant absorption increase due to surface plasmon–polariton excitation [26], while the underlying phonon-drag mechanism remains the same. Conversely, the absence of terahertz generation from thin gold films ($\lesssim$100 nm) reported in [8] follows from the absence of a directed phonon flux in the uniformly heated film. Quantitatively, for Au with $v_F \approx 1.4 \times 10^8$ cm/s and $\nu_e \sim 10^{14}\,\mathrm{s}^{-1}$ (in the moderate heating regime), the electron thermal diffusivity is $D_e \approx 70\,\mathrm{cm}^2/\mathrm{s}$. During the electron-lattice thermalization time of 1–2 ps, heat diffuses over a distance $l_d \sim \sqrt{D_e \tau_{e-\mathrm{ph}}} \approx 70 - 100$ nm. Hence, in films thinner than $\sim$ 100 nm, the lattice is heated almost uniformly and no directed phonon flux and phonon-drag force develops, so the terahertz emission is suppressed, in full agreement with the experimental observations [8].

IV. ESTIMATES FOR HIGH-FLUENCE REGIME

The analysis above assumes a phonon distribution close to thermal equilibrium. At pump fluences of about 0.1 J/cm² and higher, however, the situation changes dramatically: the overheated region emits a coherent deformation wave, which can evolve into a shock wave. As shown in molecular dynamics simulations and experiments (see, for example, [27,28]), at absorbed fluences of 0.5–1 J/cm², such a deformation wave accumulates tens of percent of the absorbed energy.

In terms of phonons, this can be viewed as the stimulated excitation of a selected phonon mode against the background of spontaneous excitation of the entire phonon spectrum, i.e., lattice heating. Microscopically, the stimulated emission originates from the fact that the probability of emitting of a phonon with a given wave vector $\mathbf{q}$ is proportional to the population of that mode [17,18].

Let us estimate the drag force for this case using macroscopic mechanical treatment. Consider the near-surface layer of the crystal lattice receiving the thermal energy $\Delta U_l = \Phi_{\mathrm{abs}}/l_d$ (per unit volume), where Φ_{abs} is the absorbed fluence and l_d is the heat diffusion length during the time of electron–lattice thermalization ($\sim$ 1 ps). The pressure increase inside the layer ΔP is given by $\Delta P = \Gamma \Delta U_l$, where Γ is the Grüneisen parameter, $\Gamma = (1 \div 3)$ for metals. The pressure relaxation takes time $\tau_s = l_d/c_s$, and during this time the layer of the density ρ obtains the velocity $v_P \cong \Delta P/\rho c_s$. Its kinetic energy per unit volume is given by

$$E_K = \frac{1}{2\rho}\left(\frac{\Delta P}{c_s}\right)^2. \tag{15}$$

The fraction of absorbed energy converted into kinetic energy is therefore

$$\eta = \frac{E_K}{\Delta U_l} = \frac{\Gamma^2}{2}\frac{\Phi_{\mathrm{abs}}}{\rho c_s^2 l_d}. \tag{16}$$

To estimate the efficiency of deformation-wave generation, we use the following parameters of metals (Au, Al, and Cu): $\rho_{\mathrm{Au}} = 19.3\ \mathrm{g/cm}^3$, $\rho_{\mathrm{Al}} = 2.7\ \mathrm{g/cm}^3$, $\rho_{\mathrm{Cu}} = 8.96\ \mathrm{g/cm}^3$; sound speed $c_s \approx (3 \div 5) \times 10^5$ cm/s; Grüneisen parameter $\Gamma \approx 2$; and heat diffusion depth $l_d \approx 30$ nm. Estimating l_d, we took into account that at high electronic temperatures $\sim$1 eV and high lattice temperatures the electron collision frequency increases about an order of magnitude (for example, up to $10^{15}\,\mathrm{s}^{-1}$ in Au [29,30]) and the thermal diffusivity decreases proportionally. Substituting these values into Eq. (16) yields $\eta \approx 10\% - 30\%$ for $\Phi_{\mathrm{abs}} \approx 0.1\,\mathrm{J/cm}^2$, which is in good agreement with Refs. [27,28].

Transformation of the pump energy directly into the deformation wave nonlinearly enhances the phonon-drag effect. The momentum carried by the deformation wave, $P_K = E_K/c_s$, is transferred to electrons with the frequency $\nu_{\mathrm{ph}-e}$, creating the drag force $F_K = \nu_{\mathrm{ph}-e} P_K$, which is predominantly normal to the surface. Compare F_K with the drag force produced by phonon diffusion (4):

$$\beta = \frac{F_K}{F_{\mathrm{ph}}} = \frac{3\Gamma^2}{2}\frac{\nu_{\mathrm{ph}}\Phi_{\mathrm{abs}}}{\rho c_s^3}. \tag{17}$$

Estimates for Au, Al, and Cu give similar results and show that the influence of the deformation wave begins to dominate (i.e., $\beta > 1$) at the absorbed fluences of 10−30 mJ/cm².

The condition of the quasistatic electron equilibrium (11) allows us to estimate electric fields generated near the metal surface. First, it gives the normal component of electric field:

$$en_e E_x = \frac{\nu_{\mathrm{ph}-e} E_K}{c_s} = \nu_{\mathrm{ph}-e}\frac{\Gamma^2 \Phi_{\mathrm{abs}}^2}{2\rho c_s^3 l_d^2}. \tag{18}$$

At the same time, the quasistatic character of the electric field leads to rot $\mathbf{E} = 0$, or under the chosen geometry, $\frac{\partial E_x}{\partial z} = \frac{\partial E_z}{\partial x}$. Replacing derivatives by reversed spatial scales (l_d along the x axis and λ_{THz} along the z axis), we finally arrive at the following expression for the tangential electric field:

$$E_z \cong \frac{\Gamma^2}{2}\frac{1}{en_e}\frac{\nu_{\mathrm{ph}-e}\Phi_{\mathrm{abs}}^2}{\rho c_s^3 l_d}\frac{2\pi}{\lambda_{\mathrm{THz}}}. \tag{19}$$

Here the spatial scale λ_{THz} is the characteristic size of the perturbed area along the z axis (see Fig. 1), which coincides with the terahertz pulse length ($\sim$ 0.3 mm). In complete analogy with Sec. III, the tangential component E_z is continuous across the metal surface and serves as the source of the emitted terahertz radiation. In Cherenkov geometry, once E_z is known, the magnetic field at the surface is obtained from the boundary condition $H_y = -E_z/\cos\alpha$, which gives the Poynting vector and the radiated power per unit area. Note that in this regime the terahertz pulse energy scales as the fourth power of the absorbed fluence. Owing to the nonlinearity of laser absorption, the dependence on the incident optical fluence is expected to be even steeper.

Apparently, this regime of terahertz generation from Cu was observed in Refs. [11,31], where the terahertz pulse energy measured by the calibrated bolometer reaches 0.2 nJ at pump fluence up to $1\,\mathrm{J/cm}^2$ (the laser pulse energy was 2.5 mJ and the estimated focal spot size on the metal surface was about 0.5 mm). For the parameters of Cu and $\Phi_{\mathrm{abs}} = 0.2\,\mathrm{J/cm}^2$, from Eq. (19) we obtain $E_z \sim 2\,\mathrm{kV/cm}$. Accounting for the geometry of the laser beam focusing described in [31], we find the terahertz pulse energy $\sim$ 0.3 nJ, which is close to the measured one.

V. CONCLUSION

In conclusion, we have proposed a mechanism for optical-to-terahertz conversion on metal surfaces based on the phonon-drag force. The phonon flux develops on picosecond timescales with the crystal lattice heating, which naturally explains the significant delay in the terahertz response. The phonon-drag model predicts the terahertz pulse duration of about 0.5–1 ps and spectral maximum at 0.3–1.5 THz, in good agreement with experiments. This result is robust against significant variations of the relaxation constants.

At high pump fluences, a macroscopic deformation wave starts to dominate over the diffusive phonon flux, which nonlinearly enhances the drag effect and modifies the terahertz generation regime. This effect establishes a connection between the ultrafast electromagnetic response of laser-irradiated metal and its macroscopic motion. According to our model, the terahertz signal reflects the initial dynamics of the deformation-wave appearance due to the crystal lattice heating and further mechanical relaxation.

Finally, we emphasize that the proposed model relies on the constants of *e–ph* and *ph–ph* interactions, and therefore admits quantitative comparison with experiment, limited only by the accuracy with which these parameters are known form measurements or first-principle calculations.

ACKNOWLEDGMENTS

The author is grateful to A. V. Korzhimanov, E. D. Gospodchikov, V. A. Mironov, and M. D. Tokman for fruitful discussions. This work was supported by the Russian Science Foundation through Grant No. 25-22-20019.

The author declares no conflict of interest.

DATA AVAILABILITY

The data that support the findings of this study were generated by numerical simulations. The source code and parameters used to generate the simulations are publicly available [32].

APPENDIX A: DERIVATION OF THE MOMENTUM EQUATIONS FOR THE BOLTZMANN EQUATION

We introduce the phonon distribution function over momenta $f_{\rm ph}(\mathbf{q}, \mathbf{r}, t)$. In this section we assume that only a small fraction of phonons participates in the formation of the directed energy flux, so that the distribution function can be treated perturbatively:

$$f_{\rm ph}(\mathbf{q}, \mathbf{r}, t) = f_0(q, \mathbf{r}, t) + \delta f(\mathbf{q}, \mathbf{r}, t), \tag{A1}$$

where f_0 is the isotropic part of the distribution, describing the total energy of the phonon subsystem (or its effective temperature) and depending only on $q = |\mathbf{q}|$, while $\delta f(\mathbf{q})$ is a small anisotropic perturbation that describes the phonon flux.

The time evolution of the full distribution function is governed by the Boltzmann kinetic equation:

$$\frac{\partial f_{\rm ph}}{\partial t} + \frac{\partial f_{\rm ph}}{\partial \mathbf{r}}\mathbf{c}_s = s_e(q, \mathbf{r}, t) + St_{th}\{f_0\} + St_U\{\delta f\} + St_{e-ph}\{f_e, f_{\rm ph}\}, \tag{A2}$$

where $s_e(q, \mathbf{r}, t)$ is the isotropic (in $\mathbf{q}$-space) source of phonon generation by hot electrons, $\mathbf{c}_s$ is the phonon velocity vector, and St_i are the collision integrals. Specifically, $St_{\rm th}\{f_0\}$ governs thermalization within the phonon subsystem via normal phonon–phonon collisions that conserve total momentum and energy; $St_U\{\delta f\}$ represents momentum loss through Umklapp *ph–ph* scattering (U processes); and $St_{e-\rm ph}\{f_e, f_{\rm ph}\}$ describes momentum exchange with the electron subsystem characterized by the distribution function f_e (its contribution is discussed below). The explicit form of the first collision integral is not required, while the second one is treated in the relaxation-time approximation as $t_m\{\delta f\} = -\nu_U\ \delta f$, where ${\nu_U}^{-1}$ is the characteristic momentum relaxation time due to U processes.

Of course, the relevant relaxation rates depend on the phonon energy and on the electron temperature; their behavior is known primarily from theoretical calculations (see, e.g., Refs. [16–18]). Typically, high-energy phonons with wave numbers approaching the Brillouin zone boundary exhibit scattering rates an order of magnitude larger than those of phonons with energies around 0.02–0.03 eV, corresponding to room temperature. In what follows, we work with the moments of $f_{\rm ph}$ (the average momentum and energy of phonons per unit volume). Since the lattice is strongly heated in the regime of interest, the relevant collision frequencies are taken to be those characteristics of high-energy phonons, which dominate the momentum exchange.

Under these assumptions, the evolution of the anisotropic perturbation δf is governed by

$$\frac{\partial \delta f}{\partial t} + \frac{\partial f_0}{\partial \mathbf{r}}\mathbf{c}_s = -\nu_U \delta f + St_{e-ph}. \tag{A3}$$

Here we have used the fact that the collision integral $St_{th}\{f_0\}$ and the source $s_e(q, \mathbf{r}, t)$ are isotropic in momentum and thus do not contribute to δf. The total phonon momentum per unit volume, $\mathbf{P}_{\rm ph}$, and the total phonon energy per unit volume, U_l (the thermal energy of the crystal lattice), are expressed in terms of δf and f_0 as

$$\mathbf{P}_{\rm ph} = \int \delta f \hbar \mathbf{q}\, d^3\mathbf{q}, \tag{A4}$$

$$U_l = \int f_0 \hbar q c_s\, d^3\mathbf{q}. \tag{A5}$$

To find the equation of $\mathbf{P}_{\rm ph}$ change, multiply the kinetic Eq. (A3) by $\hbar\mathbf{q}$ and integrate it over the whole $\mathbf{q}$ space:

$$\frac{\partial \mathbf{P}_{\rm ph}}{\partial t} + \frac{1}{3}\nabla U_l = -\nu_U \mathbf{P}_{\rm ph} + \int St_{e-ph}\hbar\mathbf{q}\, d^3\mathbf{q}. \tag{A6}$$

Here we have taken into account that the distribution function f_0 is isotropic, so the integrals of the form $\int f_0 q_i^2 \mathrm{d}^3\mathbf{q}$ are equal to each other for any projection $q_i = \{q_x, q_y, q_z\}$.

The last term in Eq. (A6) describes momentum exchange between the phonon and electron subsystems. Evidently, in the absence of directed momentum in either subsystem, this term must vanish, irrespective of whether the subsystems are

thermalized. A nonzero value of the integral can only arise from anisotropies in the electron and phonon distribution functions, which, for small perturbations, are linearly related to the momentum of the respective subsystem. In particular, if the phonon subsystem carries momentum $\mathbf{P}_{\rm ph}$, it transfers momentum to the electrons at a rate $\nu_{{\rm ph}-e}\mathbf{P}_{\rm ph}$; similarly, if the electron subsystem carries momentum $\mathbf{P}_e$, it is transferred to the phonons at a rate $\nu_{e-{\rm ph}}\mathbf{P}_e$, where $\nu_{e-{\rm ph}}$ is the electron–phonon collision frequency. We thus obtain

$$\frac{\partial \mathbf{P}_{\rm ph}}{\partial t} + \frac{1}{3}\nabla U_l = -\nu_U \mathbf{P}_{\rm ph} - \nu_{{\rm ph}-e}\mathbf{P}_{\rm ph} + \nu_{e-{\rm ph}}\mathbf{P}_e. \tag{A7}$$

Note that the collision frequencies $\nu_{e-{\rm ph}}$ and $\nu_{{\rm ph}-e}$ are related but not equal, since the concentrations of phonons and electrons generally differ. If N collisions per unit time occur in a unit volume, the exact balance relation $N = \nu_{e-{\rm ph}} n_e = \nu_{{\rm ph}-e} n_{\rm ph}$ must hold, where $n_{\rm ph}$ and n_e are the phonon and electron concentrations, respectively. At room temperature, $n_{\rm ph}$ exceeds n_e by one to two orders of magnitude, consistent with the fact that the phonon lifetime is considerably longer than the electron mean free time.

To obtain an equation for the phonon energy density U_l, we multiply the kinetic Eq. (A2) by $\hbar\omega = \hbar q c_s$ and integrate over momenta:

$$\frac{\partial U_l}{\partial t} + c_s^2 \,{\rm div}\, \mathbf{P}_{\rm ph} = S_e, \tag{A8}$$

where $S_e = \int s_e(q, \mathbf{r}, t)\hbar q c_s d^3\mathbf{q}$ is the integrated energy input from the electrons into the crystal lattice. The collision integrals $St_{th}\{f_0\}$ and $St_U\{\delta f\}$ do not contribute to Eq. (A8) because they conserve the total phonon energy. The term $c_s^2\,{\rm div}\,\mathbf{P}_{\rm ph}$ describes the contribution of lattice thermal conductivity to heat transport. In most metals, the electronic thermal conductivity exceeds the lattice thermal conductivity by one to two orders of magnitude, so this term provides only a small correction to the heat transport by electrons, which is governed predominantly by S_e and its evolution.

Equations (A7)–(A8) explicitly capture the emergence of a directed phonon flux that is delayed with respect to the heating of the phonon subsystem. As seen from Eq. (A7), the growth rate of the phonon momentum $\mathbf{P}_{\rm ph}$ is proportional to the gradient of the lattice thermal energy ∇U_l, which itself rises and decays on picosecond timescales.

APPENDIX B: GENERATION OF INTERNAL FIELDS AND THZ EMISSION BY A POTENTIAL SOURCE

The problem of low-frequency radiation from various gradient-type sources acting on conduction electrons near a metal surface has been solved in Refs. [1–5]. Below we summarize the main results of those works in a unified form.

Suppose that a potential force $\mathbf{F}(x, z, t)$ acts on the electrons per unit volume—for instance, the phonon-drag force associated with inhomogeneous heating of the crystal lattice. The electrons in a metal can be described as a fluid (using hydrodynamic equations) because the electron–electron collision rate is very high, especially at high temperatures, where the mean free path drops to a few nanometers even in good conductors. The equation describing the low-frequency motion of electrons then takes the form

$$\frac{\partial \mathbf{v}}{\partial t} = -\frac{e\mathbf{E}}{m} + \frac{\mathbf{F}}{mn_e} - \frac{\nabla p_e}{mn_e} - \nu_e \mathbf{v}, \tag{A9}$$

where $\mathbf{v}$ is the directed electron velocity, $\mathbf{E}$ is the self-consistent electric field inside the metal, ν_e is the effective electron collision frequency, and p_e is the electron pressure. In the ideal-gas model, $p_e = \frac{2}{3} n_e \varepsilon_e$, with ε_e being the average kinetic energy per electron. At room temperature and above, ν_e is determined predominantly by collisions with phonons so that $\nu_e \cong \nu_{e-{\rm ph}}$. When electrons are heated to temperatures comparable with the Fermi energy, electron–electron Umklapp scattering also contributes noticeably to ν_e.

The action of the force $\mathbf{F}$ induces a charge-separation field $\mathbf{E}$ and an electron density perturbation δn_e, related by Maxwell's equation:

$${\rm div}\,\mathbf{E} = -4\pi e \delta n_e. \tag{A10}$$

Using the continuity equation

$${\rm div}\, n_e \mathbf{v} = -\frac{\partial \delta n_e}{\partial t} \tag{A11}$$

and calculating the divergence of Eq. (A9), we find

$$\frac{\partial^2 \delta n_e}{\partial t^2} + \nu_e \frac{\partial \delta n_e}{\partial t} + \omega_p^2 \delta n_e = -\frac{{\rm div}\,\mathbf{F}}{m} + \frac{\boldsymbol{\Delta} p_e}{m}, \tag{A12}$$

where $\omega_p^2 = 4\pi n_e e/m$ is the plasma frequency and Δ is the Laplace operator. Here the background free-electron density n_e is taken to be constant, which is justified for electron temperatures below 0.5–1 eV, that is, below the threshold of significant internal ionization.

Since the plasma frequency in metals, $\omega_p \sim 10^{16}\,{\rm s}^{-1}$, exceeds by orders of magnitude both the characteristic time of $\mathbf{F}$ variations and the collision frequency ν_e, Eq. (A12) gives the following solution:

$$\delta n_e = -\frac{{\rm div}\,\mathbf{F} + \boldsymbol{\Delta} p_e}{m\omega_p^2} \cong \frac{1}{m\omega_p^2}\left(\frac{\partial^2 p_e}{\partial x^2} - \frac{\partial F_x}{\partial x}\right). \tag{A13}$$

Here we have also taken into account that the force $\mathbf{F}$ and the pressure p_e are localized in a thin near-surface layer so that $\frac{\partial}{\partial x} \gg \frac{\partial}{\partial z}$. Equation (A13) describes the electron density perturbation produced inside the metal by the force $\mathbf{F}$ and the electron pressure gradient, including their screening by charge-separation fields.

Because neither electron heat flux nor phonon flux crosses the metal surface, we have at the boundary $\frac{\partial p_e}{\partial x} = F_x = 0$. It follows that $\int_{-\infty}^{0} \delta n_e(x) dx = 0$, that is, the perturbation has the character of a distributed double layer with zero net surface charge. Accordingly, the normal component of the electric field of this layer is entirely localized within it, similar to the field of a parallel-plate capacitor.

Since the electron pressure and the phonon flux vary slowly compared with the plasma frequency, this double layer can emit radiation that leaves the surface. From Maxwell's equations we obtain

$$\nabla\,{\rm div}\,\mathbf{E} - \boldsymbol{\Delta}\mathbf{E} = -\frac{1}{c^2}\frac{\partial^2 \mathbf{E}}{\partial t^2} + \frac{4\pi}{c^2} n_e e \frac{\partial \mathbf{v}}{\partial t}. \tag{A14}$$

Here we make use of the expression for δn_e, since ${\rm div}\,\mathbf{E} = -4\pi e \delta n_e(x, z, t)$. Taking into account Eq. (A9) and the rela-

tions $\omega_p^2 \gg \nu_e$, $\frac{\partial}{\partial t}$ and $\frac{\partial}{\partial x} \gg \frac{\partial}{\partial z}$, we find

$$\frac{\partial^2 \mathbf{E}}{\partial x^2} - \frac{\omega_p^2}{\nu_e c^2}\frac{\partial \mathbf{E}}{\partial t} = -\frac{1}{n_e e} \times \left(\frac{\partial^2 (\nabla p_e - \mathbf{F})}{\partial x^2} - \frac{\omega_p^2}{\nu_e c^2}\frac{\partial (\nabla p_e - \mathbf{F})}{\partial t} \right). \tag{A15}$$

As is evident from Eq. (A15), the differential operators acting on $\mathbf{E}$ and on $(\nabla p_e - \mathbf{F})$ are identical. Hence we obtain the quasistatic solution

$$\mathbf{E} = \frac{\mathbf{F} - \nabla p_e}{n_e e}. \tag{A16}$$

The obtained solution corresponds to the quasistatic limit, i.e., zero electron velocity $\mathbf{v} = 0$ and rot $\mathbf{E} = 0$. This reflects the fact that in the dense electron plasma of a metal, any potential force is almost immediately compensated by a charge-separation field.

[1] S. A. Uryupin and A. A. Frolov, Generation of surface waves and low-frequency radiation under exposure of a conductor to a laser pulse focused by a cylindrical lens, Quantum Electron. **44**, 866 (2014).

[2] V. A. Mironov, I. V. Oladyshkin, E. V. Suvorov, and D. A. Fadeev, Generation of terahertz radiation during reflection of femtosecond laser pulses from a metal surface, J. Exp. Theor. Phys. **119**, 179 (2014).

[3] S. G. Bezhanov and S. A. Uryupin, Generation of nonlinear currents and low-frequency radiation upon interaction of a laser pulse with a metal, Quantum Electron. **43**, 1048 (2013).

[4] I. V. Oladyshkin, D. A. Fadeev, and V. A. Mironov, Thermal mechanism of laser induced THz generation from a metal surface, J. Opt. **17**, 075502 (2015).

[5] S. G. Bezhanov and S. A. Uryupin, Free-electron mechanisms of low-frequency radiation generation on metal surfaces, Opt. Lett. **41**, 4975 (2016).

[6] D. J. Hilton, R. D. Averitt, C. A. Meserole, G. L. Fisher, D. J. Funk, J. D. Thompson, and A. J. Taylor, Terahertz emission via ultrashort-pulse excitation of magnetic metal films, Opt. Lett. **29**, 1805 (2004).

[7] F. Kadlec, P. Kužel, and J.-L. Coutaz, Optical rectification at metal surfaces, Opt. Lett. **29**, 2674 (2004).

[8] F. Kadlec, P. Kužel, and J.-L. Coutaz, Study of terahertz radiation generated by optical rectification on thin gold films, Opt. Lett. **30**, 1402 (2005).

[9] G. K. P. Ramanandan, G. Ramakrishnan, N. Kumar, A. J. L. Adam, and P. C. M. Planken, Emission of terahertz pulses from nanostructured metal surfaces, J. Phys. D Appl. Phys. **47**, 374003 (2014).

[10] G. Ramakrishnan and P. C. M. Planken, Percolation-enhanced generation of terahertz pulses by optical rectification on ultrathin gold films, Opt. Lett. **36**, 2572 (2011).

[11] E. V. Suvorov, R. A. Akhmedzhanov, D. A. Fadeev, I. E. Ilyakov, V. A. Mironov, and B. V. Shishkin, Terahertz emission from a metallic surface induced by a femtosecond optic pulse, Opt. Lett. **37**, 2520 (2012).

[12] G. H. Welsh, N. T. Hunt, and K. Wynne, Terahertz-pulse emission through laser excitation of surface plasmons in a metal grating, Phys. Rev. Lett. **98**, 026803 (2007).

[13] G. H. Welsh and K. Wynne, Generation of ultrafast terahertz radiation pulses on metallic nanostructured surfaces, Opt. Express **17**, 2470 (2009).

[14] Y. G. Gurevich and O. L. Mashkevich, The electron-phonon drag and transport phenomena in semiconductors, Phys. Rep. **181**, 327 (1989).

[15] S. Kazemian and G. Fanchini, Nickelocene SPM tip as a molecular spin sensor, J. Phys.: Condens. Matter **37**, 095802 (2025).

[16] C. Kittel, *Introduction to Solid State Physics*, 8th ed. (Wiley, New York, 2018), Chap. 5.

[17] U. Ritzmann, P. M. Oppeneer, and P. Maldonado, Theory of out-of-equilibrium electron and phonon dynamics in metals after femtosecond laser excitation, Phys. Rev. B **102**, 214305 (2020).

[18] Z. Tong, S. Li, X. Ruan, and H. Bao, Comprehensive first-principles analysis of phonon thermal conductivity and electron-phonon coupling in different metals, Phys. Rev. B **100**, 144306 (2019).

[19] L. D. Landau and E. M. Lifshitz, *Statistical Physics*, 3rd ed. (Elsevier, 2013), Chap. 5.

[20] S. Ono, Thermalization in simple metals: Role of electron-phonon and phonon-phonon scattering, Phys. Rev. B **97**, 054310 (2018).

[21] S. I. Anisimov, B. L. Kapeliovich, and T. L. Perel'man, Electron emission from metal surfaces exposed to ultrashort laser pulses, Sov. Phys. JETP **39**, 375 (1974).

[22] P. B. Allen, Theory of thermal relaxation of electrons in metals, Phys. Rev. Lett. **59**, 1460 (1987).

[23] N. W. Ashcroft and N. D. Mermin, *Solid State Physics* (Holt, Rinehart and Winston, 1976), Chaps. 1 and 14.

[24] I. E. Ilyakov, B. V. Shishkin, D. A. Fadeev, I. V. Oladyshkin, V. V. Chernov, A. I. Okhapkin, P. A. Yunin, V. A. Mironov, and R. A. Akhmedzhanov, Terahertz radiation from bismuth surface induced by femtosecond laser pulses, Opt. Lett. **41**, 4289 (2016).

[25] J. Dai and X.-C. Zhang, Terahertz wave generation from thin metal films excited by asymmetrical optical fields, Opt. Lett. **39**, 777 (2014).

[26] I. V. Oladyshkin, D. A. Fadeev, and V. A. Mironov, Optical excitation of surface plasmons and terahertz emission from metals, Phys. Rev. B **100**, 085421 (2019).

[27] B. J. Demaske, V. V. Zhakhovsky, N. A. Inogamov, and I. I. Oleynik, Ultrashort shock waves in nickel induced by femtosecond laser pulses, Phys. Rev. B **87**, 054109 (2013).

[28] M. B. Agranat, S. I. Anisimov, S. I. Ashitkov, V. V. Zhakhovskii, N. A. Inogamov, P. S. Komarov, A. V. Ovchinnikov, V. E. Fortov, V. A. Khokhlov, and V. V. Shepelev, Strength properties of an aluminum melt at extremely high tension rates under the action of femtosecond laser pulses, JETP Lett. **91**, 471 (2010).

[29] C. Fourment, F. Deneuville, D. Descamps, F. Dorchies, S. Petit, O. Peyrusse, B. Holst, and V. Recoules, Experimental

determination of temperature-dependent electron-electron collision frequency in isochorically heated warm dense gold, Phys. Rev. B **89**, 161110(R) (2014).

[30] Z. Chen *et al.*, Ultrafast multi-cycle terahertz measurements of the electrical conductivity in strongly excited solids, Nat. Commun. **12**, 1638 (2021).

[31] R. A. Akhmedzhanov, I. E. Ilyakov, V. A. Mironov, I. V. Oladyshkin, E. V. Suvorov, D. A. Fadeev, and B. V. Shishkin, Generation of terahertz radiation by interaction of intense femtosecond laser pulses with a metal surface, Radiophys. Quantum Electron. **57**, 807 (2015).

[32] https://github.com/oladyshkin/PhononDrag_THz.